Reaction Kinetics, Mechanisms and Catalysis (2024) 137:2019–2035
https://doi.org/10.1007/s11144-024-02639-5

Biomass high energy density fuel from oleoresin-based turpentine: catalytic hydrogenation conversion and properties in blends with fossil jet fuel

Lixin Qu[1] · Hongzhao Xie[2] · Xiaopeng Chen[1] · Shen Luo[1] · Xiaoying Tang[1] · Jiezhen Liang[1] · Xiaojie Wei[1] · Linlin Wang[1]

Received: 20 February 2024 / Accepted: 23 April 2024 / Published online: 9 June 2024

Abstract

The carboxylic multi-walled carbon nanotube-loaded nickel (Ni/c-MWCNT) catalyst prepared by the excess impregnation method was used for the hydrogenation of oleoresin-based turpentine (OBT) into high energy density fuel. Benefiting from small nickel nanoparticle sizes (about 10 nm) and the carrier's high surface area, a hydrogenation rate of 99.1% was achieved at 145 °C and 3 MPa, superior to a commercial 5 wt.% Pd/C. Hydrogenated oleoresin-based turpentine (HOBT) satisfied the density, flash point, and freezing point outlined by the American Society of Testing and Materials standard. Hydrogenation improved the oxidative stability, smoke point, and calorific value of OBT while changing its color to water white. The impact of blend ratio on the blended biomass fuel performance was evaluated by measuring the smoke point, density, kinematic viscosity, calorific value, freezing point, and flash point of biofuels blended with HOBT and exo-tetrahydrodicyclopentadiene (JP-10). When HOBT was blended up to 20% (v/v) with JP-10, the performance of blended biomass fuel was comparable to that of JP-10 and even superior at freezing temperatures.

✉ Linlin Wang
wanglinlin1971@sina.com

[1] School of Chemistry and Chemical Engineering, Guangxi Key Laboratory of Petrochemical Resources Processing and Process Intensification Technology, Guangxi University, Nanning 530004, People's Republic of China

[2] Guangxi Standardization Association, Nanning 530009, People's Republic of China

Graphical abstract

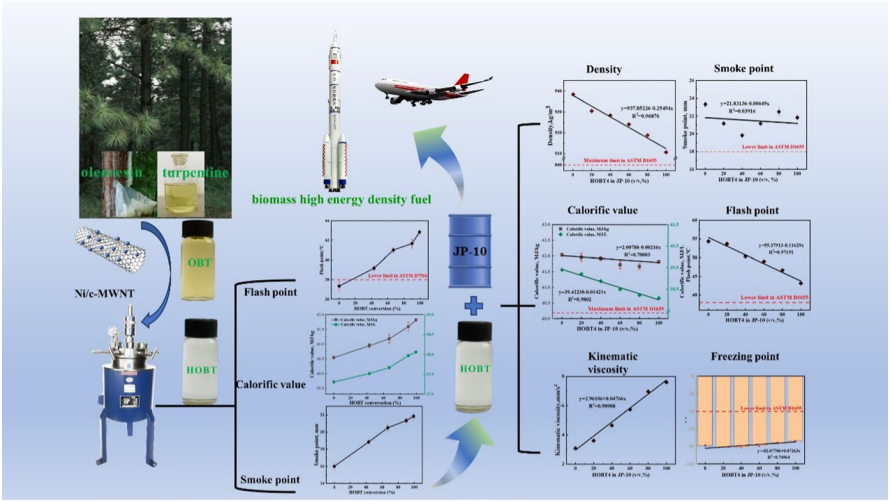

Keywords Oleoresin-based turpentine (OBT) · Hydrogenated oleoresin-based turpentine (HOBT) · High energy density · Carboxylated multi-walled carbon nanotube-loaded nickel (Ni/c-MWCNT) · Biomass fuel · Blend

Introduction

High energy density (density greater than 850 kg/m^3 at 20 °C and volumetric calorific value upwards of 36.0 MJ/L) is vital regarding an aerospace vehicle's flight range and payload capacity because the high density and volumetric net heat of combustion can bestow aircraft with augmented range and load-bearing capacity for a given fuel tank volume [1, 2]. Compared with other fuels, the density of exo-tetrahydrodicyclopentadiene (JP-10) can reach 936 kg/m^3 and offers notable performance benefits regarding freezing point and viscosity. However, these fuels are derived from fossil resources. To alleviate the pressure of depleting finite oil reserves and to achieve the goal of carbon neutrality, there is a need to develop sustainable and environmentally friendly high energy density biomass fuels [3].

Turpentine is a natural product obtained by distilling oleoresin from live pine trees. The pinus tree genus is found almost worldwide, most commonly in Asia, Europe, North America, Mediterranean Africa, and different island countries [4]. Approximately 0.6 million tons of oleoresin were produced yearly in China [5], and 350 kt of turpentine were produced worldwide [6]. Oleoresin consists mainly of non-volatile rosin (cyclic resin acid C20) and a small amount of volatile turpentine (cyclic terpenes C10 and C15). Turpentine is composed primarily of the monoterpenes (C10) α-pinene and β-pinene, with lesser amounts of carene and camphene, as well as small quantities of sesquiterpenes (C15) such

as caryophyllene and longifolene. Some studies have shown that as a potential renewable fuel, turpentine can be blended with diesel [7] or petrol [8] with minimal or no adjustments to the engine. However, owing to the affluent unsaturated hydrocarbons (carbon–carbon double bond), which hurt both sooting tendency and fuel stability, turpentine is unsatisfactory as a direct constituent of jet fuel [9, 10].

Hydrogenation is a promising approach that can alter the hydrocarbon composition to saturation, and therefore, an improvement in the sooting tendencies and oxidative stability of jet fuel can be achieved [11, 12]. In contrast to catalytic hydrogenation, electrochemical hydrogenation does not require hydrogen. However, it necessitates separating the product from the electrolyte, which can result in lower process economics [13]. Therefore, most hydrogenation reactions still use traditional methods. The performance of hydrogenated turpentine with hydrogenation by Pt/Al_2O_3 catalyst and oxygenated turpentine was analyzed and compared in diesel fuel applications [14]. A 5 wt.% Pd/C was used as a catalyst to hydrogenate turpentine, and the hydrogenated turpentine's gaseous and particle matter emissions and combustion analysis were compared with those from diesel fuel [15]. Currently, the focus of turpentine hydrogenation in preparing renewable fuel is mainly on the properties of hydrogenated turpentine as various fuels, including diesel, gasoline, and jet fuel. The catalytic hydrogenation process also predominantly uses precious metal catalysts such as Pd-based and Pt-based catalysts. Therefore, it is desirable to develop an inexpensive Ni-based catalyst of turpentine to jet fuel under relatively mild reaction conditions.

Turpentine's high calorific value, low viscosity, and low boiling point enable efficient fuel atomization and vaporization, resulting in improved exothermic rates [16]. However, the density of approximately 860 kg/m^3 falls significantly short of high-density fuels, which possess densities surpassing 900 kg/m^3. Compared with monoterpenes C10, diterpenes C20 possessing a 3-ring configuration could be more encouraging substrates for fabricating dense, sustainable aviation fuels [17]. However, oleoresin has poor properties, such as low viscosity and calorific value. Using oleoresin-based turpentine (OBT) as feedstocks to prepare high-density hydrocarbon jet fuels would exhibit intriguing potential.

In summary, no reports specifically address the catalytic hydrogenation of OBT to create high energy density fuel oil from biomass. In this work, high-density oleoresin of Masson pine (*Pinus massoniana* Lamb.) was blended with low-viscosity, high-calorific-value turpentine of Masson pine in varying ratios to achieve the performance of JP-10. The Ni/c-MWCNT catalyst prepared by excess impregnation was used to hydrogenate OBT. The catalyst achieved 99.1% hydrogenation of OBT at 145 °C, 3 MPa H_2, and 1 h, whereas the hydrogenation rate of a commercial 5 wt.% Pd/C catalyst under the same conditions was only 92.8%. Gas chromatography-mass spectrometry (GC–MS) was used to study the composition of OBT and hydrogenated oleoresin-based turpentine (HOBT) to calculate the hydrogenation rate. The effects of hydrogenation and compounding on the performance of blended biomass fuels were investigated using color, smoke point, density, kinematic viscosity, calorific value, flash point, and freezing point as the main parameters, and the potential of HOBT as a high-energy–density renewable biomass aviation fuel was assessed.

Material and methods

Materials

The c-MWCNTs (outer diameter of 5–15 nm and length of 10–30 μm, purity 96 wt.%) were purchased from Chengdu Jiacai Technology Co., Ltd. Oleoresin of Masson pine was newly collected in Dadeng Village, Santang Town that year. Turpentine of Masson pine was purchased from Guangxi Wuzhou Richeng Forest Products Chemical Co., Ltd. Superior pure polyvinyl pyrrolidone K30 (PVP) was purchased from Sinopharm Chemical Reagent Co., Ltd. Analytically pure $Ni(NO_3)_2{\cdot}6H_2O$ was bought from the Guangdong Provincial Chemical Reagent Engineering Technology Research and Development Centre.

Catalysts preparation

Catalysts were prepared using the excess impregnation method. The 0.6 g of c-MWNTs were added to water containing 0.013 g PVP and stirred by magnetic force for 2 h at room temperature. Next, the 1.27 g $Ni(NO_3)_2{\cdot}6H_2O$ was dissolved in deionized water and added to the mixture of c-MWCNTs and PVP. The mixture was stirred further at room temperature using a magnetic agitator for 4 h. The excess water was removed using a rotary evaporator. After that, it was dried in an oven at 100 °C for 24 h. Finally, the Ni/c-MWCNT catalyst with a 30% nickel loading was acquired through reduction at 350 °C for 3 h under an argon gas environment with 5% hydrogen concentration. The process is shown in Fig. S1.

Catalyst characterization

The Scanning Electron Microscope (SEM) used for SEM characterization was a GeminiSEM360. Ni/c-MWCNT was harder to disperse in water. It was transferred to a tube containing anhydrous ethanol for ultrasonic dispersion to prevent the catalyst from oxidizing and achieve more efficient dispersion. Finally, the sample was deposited on the conductive glue to create the sample.

Crystal structure information of catalysts was identified in a Bruker D8 X-ray diffractometer. The experiment was conducted using Cu-Kα radiation with a wavelength of 0.154 nm. The voltage and current used were 40 kV and 40 mA. The scanning angle covered a range from 5° to 90°. Powder samples were placed horizontally onto a slide surface previously cleaned by alcohol and flattened with another slide.

The TG209 F3 thermogravimetric (TG) analyzer determined the active metal loading of the catalysts. After reduction, a 5 mg sample of the catalyst was taken into a ceramic crucible, heated to 40 °C and maintained for 20 min, followed by a thermogravimetric analysis. During the experiment, the temperature was varied between 40 °C and 850 °C with a heating rate of 10 °C/min. An air atmosphere was employed, and the airflow rate was maintained at 30 mL/min.

Feedstock selection and hydrogenation

Oleoresin and turpentine were mixed in mass ratios of 1.5:1, 1:1, 1:1.5, and 1:2. The oleoresin and turpentine mixture was heated to 95 °C to dissolve the oleoresin completely. The mixture was filtered to eliminate impurities before the measurements of density, kinematic viscosity, and calorific value.

A process of hydrogenation is shown in Fig. S2. The hydrogenation of OBT was performed in a 100 mL stainless-steel autoclave equipped with a temperature, pressure, and speed controller. A specific portion of OBT was added to the autoclave, with a catalyst representing 5% of the oleoresin's weight in the feedstock. Next, a circulating water multi-purpose vacuum pump was used to evacuate the air in the autoclave and reduce the pressure to 0.009 MPa, which was maintained for 5 min. The autoclave's pressure was raised to 2 MPa and maintained for 5 min to ensure tightness. The pressure in the autoclave was released to 0.5 MPa, then raised to 2 MPa, and switched three times back and forth to completely displace the air in the vessel, and the last time the pressure was still held at 2 MPa. Next, the reaction system was heated while stirring constantly at 200 rpm. Once the pre-set temperature was achieved, the stirring speed was increased to 500 rpm to initiate the reaction. The pressure was consistently maintained at the set level using a hydrogen cylinder during the response.

At the end of the hydrogenation process, the temperature was lowered, and the pressure was released; the catalyst was removed by filtration to produce the final liquid product. HOBT with 43%, 67%, 90%, and 99.1% hydrogenation were synthesized by controlling the hydrogenation time and were designated HOBT1, HOBT2, HOBT3 and HOBT4.

GC–MS analysis

The OBT and HOBT underwent qualitative analysis by Agilent GC–MS 7890A-5975C gas chromatography-mass spectrometry, which employed a capillary column of HP-5MS with dimensions of 30 m in length, 0.25 mm in diameter, and 0.25 μm in film thickness. The injection temperature utilized was 540 K. High-purity nitrogen was used as the carrier gas with a split ratio of 25:1, and the injection volume was 0.4 μL. The heating procedure comprised of the following: increasing from 338 to 353 K at a rate of 3 K/min, followed by a rate of 20 K/min to 433 K, then 8 K/min to 493 K, 1 K/min to 503 K, and finally 20 K/min to 523 K, then maintain this temperature for 3 min. The obtained mass spectra underwent screening against a database, and characterization was performed using HOBT as per the pertinent literature.

The HOBT was quantitatively analyzed using an Agilent GC7820A meteorological gas chromatograph (DB-5: 30 m × 0.25 mm × 0.25 μm, FID). The GC ramping process was identical to that of GC–MS, with component contents calculated using area normalization. The hydrogenation rate in the reaction of OBT is determined by the conversion of pinene and abietic acid, as shown in Eq. 1.

$$X = \frac{W_{A0} - W_{A1} + W_{B0} - W_{B1}}{W_{A0} + W_{B0}} \times 100\% \quad (1)$$

W_{A0} Percentage sum of α-pinene and β-pinene in OBT. W_{A1} Percentage sum of α-pinene and β-pinene in HOBT. W_{B0} Percentage sum of palustric acid, abietic acid and neoabietic acid in OBT. W_{B1} Percentage sum of palustric acid, abietic acid and neoabietic acid in HOBT.

Characterization of biomass fuel and its blends

The sample's color change before and after hydrogenation was measured using a Gardner colorimeter, following standard ASTM D1544-2004.

The density was measured at 20 °C using a 10 mL capillary plug pycnometer based on the standard ASTM D891-18.

According to the kinematic viscosity measurement method of ASTM D445, the glass capillary viscometer was used to measure the viscosity at 20 °C. Capillary viscometers with different inner diameters were used according to the sample kinematic viscosity to ensure the reliability of the results.

The flash point was measured by SC-261 closed flash point tester following standard ASTM D93.

The freezing point was determined by implementing liquid nitrogen as a coolant with the ASTM D2386 standard. The thermometers utilized in the standard, with a temperature range of − 80–20 °C, have been substituted with thermometers that possess a temperature range of – 90–30 °C.

The smoke point was measured in a standardized lamp according to standard ASTM D1322.

The calorific value was measured at room temperature using the SHR-15B heat of combustion experiment device.

Results and discussion

Characterization of Ni/c-MWCNT catalysts

The specific surface area of catalyst is a crucial macroscopic physical property that affects the catalyst's activity and lifetime. Table S1 displays the physical and chemical properties and hydrogenation rate of the blank carrier c-MWCNT and catalyst reduced at different temperatures (350 °C-Ni/c-MWCNT and 450 °C-Ni/c-MWCNT). Table S1 demonstrates that c-MWCNT has an external surface area of up to 275.7 $m^2\ g^{-1}$, which offers a loading advantage and aids in the dispersion of active metals. The external surface area and pore volume of c-MWCNT decreased after loading with metal active ingredients. This may be due to the presence of Ni and NiO on the surface or in the pores of the carrier [18]. The 350 °C-Ni/c-MWCNT exhibited higher external surface area and hydrogenation rate than the 450 °C-Ni/c-MWCNT.

It can be seen that the high external surface area of c-MWCNT allows the catalyst to have good hydrogenation activity, which is due to the significant reduction of the mass transfer limitations that dominate the liquid-phase reaction, inducing the transport of the reactants from the bulk of the liquid to the external surface of the catalyst [19].

Fig. 1 illustrates the X-ray diffraction (XRD) profiles of c-MWCNT, 350 °C-Ni/c-MWCNT, and 450 °C Ni/c-MWCNT catalyst. The peaks observed at 24.94° (002) and 42.49° (100) pertain to carbon nanotubes. The XRD profile of 450 °C-Ni/c-MWCNT observed diffraction peaks located at 43.86°, 51.29°, and 75.83°, which were attributed to the (111), (200), and (220) crystal planes of Ni, indicating the presence of Ni loaded onto the c-MWCNT [20]. The XRD curves of 350 °C-Ni/c-MWCNT observed diffraction peaks consistent with NiO at 36.42° (111), 62.05° (220), and 78.00° (311) in addition to Ni peaks [21]. The results showed that both NiO and Ni coexist at 350 °C-Ni/c-MWCNT. Combined with the activity evaluation of the catalysts, it is evident that the synergistic effect of NiO and Ni led to a more muscular catalytic activity of 350 °C-Ni/c-MWCNT [22]. Finally, the average particle size of NiO and Ni in the catalyst was calculated according to Scherrer's formula [23], and the Scherrer equation was acquired using Eq. (2):

$$D = \frac{k\lambda}{\beta \cos\theta} \tag{2}$$

Here k is a constant with a value of 0.89, λ represents the X-ray wavelength ($\lambda = 0.154056$ nm), θ indicates the diffraction peak angle, and β denotes the half-peak width of the observed diffraction peak. Consequently, the catalyst's mean sizes of Ni and NiO particles were 10.3 and 11.2 nm.

Fig. 2 shows the TG of Ni/c-MWCNT catalysts in the air atmosphere. The alteration in the catalyst mass could be categorized into three zones. The initial stage occurred at temperatures below 200 °C, where a minor mass reduction was attributed to the escalation in temperature that eliminates the low level of water adsorbed

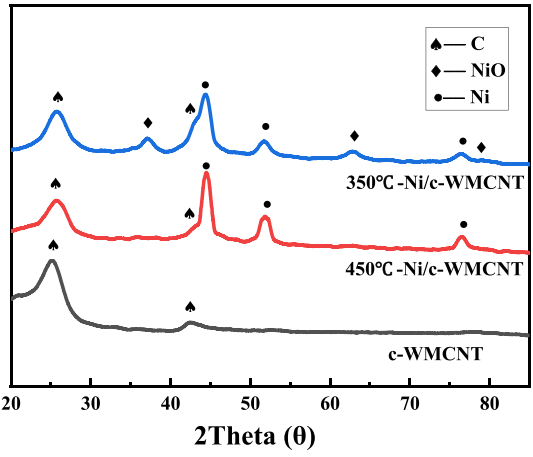

Fig. 1 XRD patterns of c-MWCNT, 350 °C-Ni/c-MWCNT and 450 °C Ni/c-MWCNT

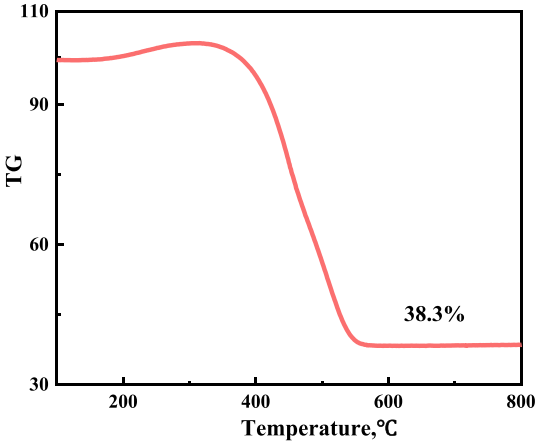

Fig. 2 TG curve of 350 °C-Ni/c-MWCNT

within the catalyst [24]. The second region, ranging from 200 °C to 350 °C, exhibited slight weight gain due to the oxidation of Ni by atmospheric oxygen, resulting in the formation of NiO. In the third region, when the temperature exceeded 350 °C, the thermal decomposition of carbon nanotubes caused a significant reduction in the overall mass, resulting in a final loss of 61.7%. At the end of the TG analysis, a residual weight percentage of approximately 38.3% indicated the amount of nickel oxide, and obtaining the nickel oxide content, the loading amount of nickel could be obtained by conversion [25, 26]. The weight percentage of nickel was calculated to be 30.0%.

The morphology and elemental composition of the Ni/c-MWCNT catalyst were studied via SEM–EDS analysis. SEM image (Fig. 3a) revealed the presence of c-MWCNTs with a nanotube structure of 5–15 nm in diameter. Ni particles were loaded onto the surface of carbon nanotubes without significant aggregation. It was consistent with the information observed in the literature [27]. Additionally, energy spectrum analysis results, depicted in Fig. 3b–d, validated the presence of C, O, and Ni in the catalyst. Moreover, the catalyst tended to have a uniform Ni and O distribution across the carrier.

The above characterization shows that the high outer surface area of c-MWCNTs allows the particle size to remain small even when nickel is heavily loaded on them.

The above characterization indicates that the high external surface area and pore structure of c-MWCNT reduces the mass transfer limitation in the liquid-phase reaction, which allows the small-sized nickel oxide and nickel loaded on it to better contact with the reactants and exhibit synergistic effects leading to the catalysts exhibiting good hydrogenation activity.

Selection of raw materials

The appropriate proportion of OBT as a biomass feedstock was determined by comparing the fuel properties of different proportions of the blends. The density, kinematic viscosity, and calorific value of OBT at different ratios are shown in Fig. S3.

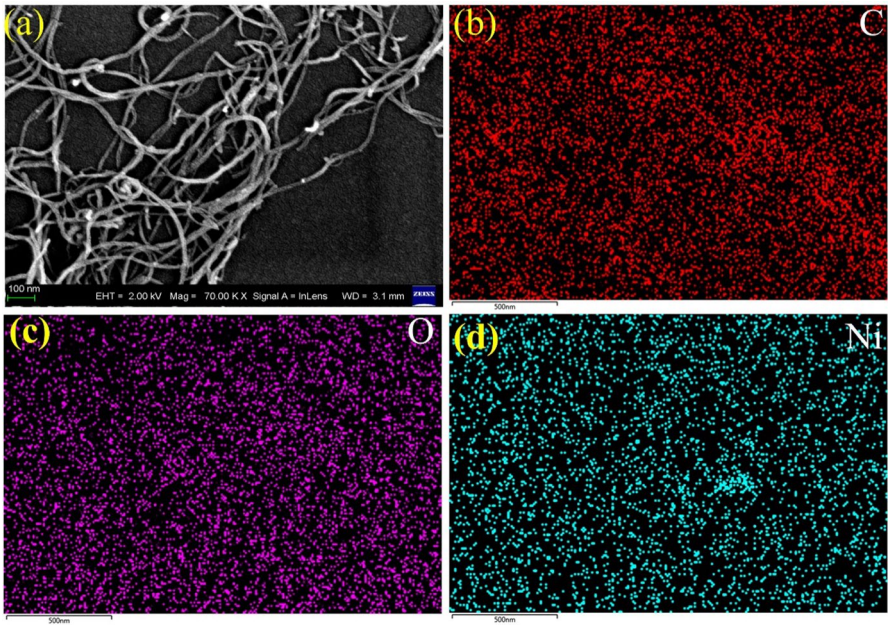

Fig. 3 SEM (**a**) and EDS (**b–d**) images of 350 °C-Ni/c-MWCNT catalyst

When the proportion of oleoresin was raised from a 1:1 ratio to 1.5:1, the mixture's density peaked at 971 kg/m^3, and the kinematic viscosity increased over three times its original value. Compared to pinene (C10) in turpentine, the abietic acid (C20) in oleoresin has more carbon molecules and a more cyclic structure. As the number of molecules increases, the fuel's density and viscosity also increase [28]. In contrast, the addition of oleoresin is worth the decrease in the calorific value of the mixture. Because the calorific value of oleoresin is only 34.9–37.2 MJ/kg, which is lower than that of turpentine [29]. As the proportion of turpentine increased, the density and kinematic viscosity of the OBT decreased gradually while the calorific value steadily increased. When the ratio of oleoresin to turpentine exceeded 1:2, the density was likely to drop below 900 kg/m^3. At this point, there was a deceleration in both the increase of calorific value and the decrease of viscosity. Therefore, OBT, an oleoresin to turpentine ratio of 1:2, was ultimately chosen as the feedstock for biomass fuel.

In conclusion, using oleoresin directly as a feedstock for jet fuel production not only increases fuel density by utilizing the C20 fraction of oleoresin but also reduces energy consumption and preparation costs for distilling turpentine from oleoresin.

Optimization of reaction conditions for hydrogenation of OBT

Univariate hydrogenation reactions of OBT were conducted to investigate the effect of each factor individually, such as catalyst amount, reaction time,

temperature, and H_2 pressure. Optimization of reaction variables ensures that resources are maximized and feedstock hydrogenation rates are significantly increased. Fig. 4 shows the effect of various factors on the hydrogenation rate of OBT. When a 5% catalyst was used, with the temperature raised to 145 °C and pressure set to 3 MPa for 60 min, the hydrogenation rate increased dramatically to 99.1%.

There was not much room for the hydrogenation rate to increase when the conditions were raised afterward. The above conditions were set as the optimal reaction conditions while maximizing the use of resources. Hydrogenation rates of merely 92.8% were attained using a commercial 5 wt.% Pd/C catalyst under the same conditions. To sum up, compared to conventional hydrogenation of abietic acids and terpenes over Pd-based catalysts, in this work, high loading and small reactive metal particle size loaded non-precious metal catalyst was synthesized using large surface c-MWCNT as carriers, and a hydrogenation rate was achieved to 99.1% at more moderate 145 °C and 3 MPa which superior to commercial 5 wt.% Pd/C.

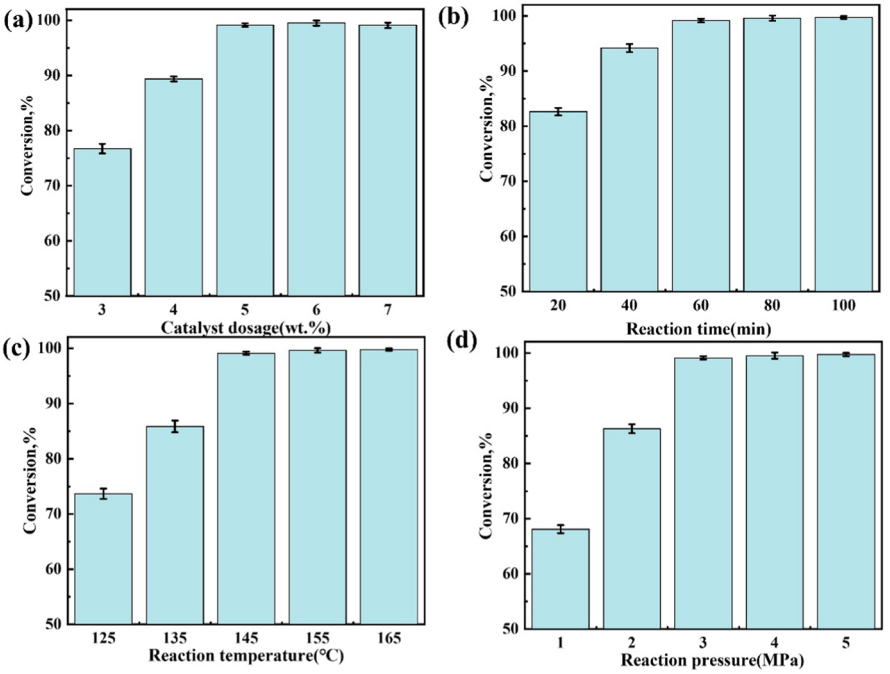

Fig. 4 **a** Effect of catalyst dosage on the OBT hydrogenation rate, reaction condition: H_2 3 MPa, 60 min, 145 °C. **b** Effect of reaction time on OBT hydrogenation rate, condition: H_2 3 MPa, 5% Ni/c-MWCNT, 145 °C. **c** Effect of reaction temperature on the OBT hydrogenation rate, reaction condition: H_2 3 MPa, 5% Ni/c-MWCNT, 60 min. **d** Effect of reaction pressure on OBT hydrogenation rate, condition: 5% Ni/c-MWCNT, 60 min, 145 °C

Composition

Commercial or military jet fuels typically have carbon numbers ranging from C8 to C16 [30]. Higher-density hydrocarbon fuels cycloalkane have higher density and heat of combustion [31]. The OBT, consisting mainly of cyclic terpene hydrocarbon monoterpenes (C10) like pinene, sesquiterpenes (C15) such as longifolene, caryophyllene, and diterpene resin acids (C20) with cyclic backbones, is a potential feedstock for jet fuel or high-density hydrocarbon fuels. Diterpene resin acid comprises multiple variations of abietic acids with the chemical formula $C_{20}H_{30}O_2$.

The unsaturated double bonds in OBT are chemically reactive and become unstable when exposed to oxygen, heat, metal ions, and light, resulting in performance degradation due to thermodynamic instability [32]. Hydrogenation of OBT entails mainly converting pinene to pinane and various types of abietic acid to hydrogenated abietic acid. Hydrogenation markedly improves the stability of OBT by transforming the unsaturated double bonds in its structure into single bonds. The abietic acid molecule can easily absorb one mole of hydrogen to form dihydroabietic acid. However, the second pair of double bonds were more resistant to hydrogenation and required harsher conditions to continue the conversion to tetrahydroabietic acid. The rate constant for reaction value for the generation of dihydroabietic acid was higher than that of tetrahydroabietic acid, while the activation energy was reversed, confirming that the generation of dihydroabietic acid was faster than that of tetrahydroabietic acid [33, 34]. Therefore, the hydrogenation products of diterpene acid consist mainly of dihydroabietic acid and a small amount of fully hydrogenated tetrahydroabietic acid. The primary hydrogenation reaction is shown in Fig. S4.

Ultimately, HOBT4, which possesses the highest hydrogenation rate, is combined with JP-10 to mitigate the effect of double bond instability on the fuel. The quantitative hydrogenation of α-pinene and dipentene was mentioned in the literature as early as 1930 [35]. However, most oleoresin components are isomers with comparable physicochemical properties, making their separation and identification challenging with previous methods. Therefore, GC–MS and GC were used for qualitative and quantitative analysis directly of the raw materials and mixture products. The GC–MS of HOBT4 is shown in Fig. S5. In Fig. S5, 5–8 are isomers of dihydroabietic acid with the same molecular formula $C_{20}H_{32}O_2$.

Table 1 Composition of HOBT4 by GC–MS

	Component	molecular formula	Composition/wt.%
1–2	Pinane	$C_{10}H_{18}$	53.80
3	Longifolane	$C_{15}H_{26}$	2.22
4	Caryophyllane	$C_{15}H_{26}$	1.74
5–8	Dihydroabietic acid	$C_{20}H_{32}O_2$	19.67
9	Tetrahydroabietic acid	$C_{20}H_{34}O_2$	5.31

The main components in HOBT4 are shown in Table 1. The results indicated that the content of pinane was 53.8%, whereas dihydroabietic acid and tetrahydroabietic acid were 19.67% and 5.31%. Overall, pinane was the dominant compound in HOBT.

Color

The ASTM D1655 does not specify color requirements for the fuel. Nevertheless, the fuel should ideally appear water-white to pale yellow in ordinary circumstances with no out-of-the-ordinary color deposits. The color change of OBT after hydrogenation is demonstrated in Fig. S6. The chromaticity of colors from left to right is 3, 3, 2, 1, 1, as per Gardner standards. Biomass fuel color gradually lightens with increasing hydrogenation rate. The clarified solution of OBT was bright yellow, which became lighter after hydrogenation and finally became water white. At this stage, the color of the mixed solution is a valuable indicator of quality and the degree of hydrogenation.

Smoke point

Smoke point is a feature of fuel combustion that leads to soot production. There is no specified smoke point limit for synthetic hydrocarbons, according to ASTM D7566. However, fuels with higher smoke points tend to smoke less, indicating superior combustion properties. Terpenes containing oxygen can inhibit soot formation, but at the same time, structural features in terpenes (e.g., double bonds and rings) promote soot formation [36].

As shown in Fig. S7a, the smoke point of OBT at different hydrogenation rates. The smoke point of OBT rose gradually with an increasing hydrogenation rate, from 16 mm to 21.8 mm, an increase of 36.3%. Hydrogenation substantially lowers the smoking tendency of the fuel, thereby rendering biomass fuel cleaner and more environmentally friendly. The same conclusion was reached in the literature [37]. To eliminate the impact of sooting tendencies and fuel stability, the HOBT4 with the highest hydrogenation rate was blended with JP-10 in ratios of 20%, 40%, and 60%, 80% by volume. The blend biomass fuel demonstrated anti-synergistic properties at 20%, 40%, and 60% HOBT4 content in the blend, resulting in lower overall fuel performance than the individual fuel (see Fig. S7b).

Density

For limited-sized aerial vehicles, high-density fuels enable greater payload and increase the aircraft's range without altering tank capacity [38]. This is due to the impact of density on the fuel's volumetric calorific value. The density of the OBT was 920 kg/m^3, significantly surpassing the ASTM D7566 requirement. The abietic acid in the OBT could increase density due to the hydrophenanthrene rings, which were believed to have cycloaliphatic and aromatic structures [39]. Long-chain

(> C15) hydrocarbons such as n-alkanes, iso-alkanes, cycloalkanes, and aromatics are essential factors in increasing fuel density [40].

The density of HOBT declined as the hydrogenation rate increased, from 921 kg/m^3 to 911 kg/m^3, a decrease of 1.1%, as shown in Fig. S8a. As anticipated, density decreases as unsaturation decreases; in other words, hydrocarbon fuels with higher H/C ratios exhibit lower density [41]. The density of the blended biofuel decreased linearly as the HOBT4 content increased (see Fig. S8b) when measured at a temperature of 20 °C. Although hydrogenation reduces density, the resulting density remains above 900 kg/m^3, comparable to JP-10.

Calorific value

High calorific value is a crucial characteristic of jet fuel, as it delivers more incredible propulsive energy, resulting in enhanced flying range for aircraft. Fig. S9a displays the fluctuation of the calorific value in HOBT across four conversion levels. There was a considerable rise in calorific value as the hydrogenation rate increased, from 40.5 MJ/kg to 41.8 MJ/kg, an increase of 3.2%, resulting from an increased H/C molar ratio in OBT [42]; the effect of the H/C molar ratio on fuel density is the exact opposite of this. Hydrogenating OBT primarily involves converting pinene into pinane and abietic acid into hydrogenated abietic acid. These isomeric abietic acids contain two double bonds. If a catalyst is used to produce more tetrahydroabietic acid, the calorific value of the product significantly increases due to the large number of hydrogen atoms added. The heating values gap between OBT and commercial fuels could be narrowed using hydrogenation.

The calorific value of blends containing HOBT4 and JP-10 decreased as the amount of HOBT4 increased (see Fig. S9b). When the proportion of HOBT4 was higher, the calorific value of the blends was marginally lower than that of pure HOBT4, and a mild anti-synergistic effect was detected. The conversion of mass calorific value to volumetric calorific value indicated a linear decrease with increased HOBT. It was primarily due to the influence of two factors on volumetric calorific value: density and mass calorific value. When the content of HOBT4 reached 20%, the blended biofuel yielded a calorific value total of 39.1 MJ/L, with a slight 0.4 MJ/L variance compared with JP-10.

Low-temperature fluidity

The low-temperature flow of aviation fuel, typically evaluated based on its freezing point and kinematic viscosity [43], plays a crucial role in the ability of aircraft to fly successfully under extreme conditions, such as low temperatures and high altitudes. Excellent low-temperature flow characteristics prevent fuel crystals from clogging fuel lines and mitigate the problems of poor atomization and ignition failure caused by excessive kinematic viscosity at high altitudes. Turpentine, which can be used as a biomass fuel, has good cold flow properties and can even be prepared as a cold flow improver for other fuels [44].

After hydrogenation, OBT increased in both kinematic viscosity and freezing point (see Fig. S10a and Fig. S11a). Specifically, the kinematic viscosity displayed a clear linear trend with increasing hydrogenation rate, from 7.4 mm^2/s to 7.6 mm^2/s, a 2.7% improvement, which could be attributed to the increase in saturation [45]. Hydrogenation had a similarly negative impact on the freezing point of the OBT and became more significant with increasing hydrogenation rate, from − 80.3–− 73.3 °C, an increase of 8.7%. However, the freezing point of − 73 °C was significantly higher than the required − 40 °C specified by ASTMD 7566 and was close to JP-10.

The low-temperature fluidity of the blended fuel varies with the HOBT4 content demonstrated in Fig. S10b and Fig. S11b. The kinematic viscosity of JP-10 mixed with HOBT4 rose in a straight line with the increase in HOBT4. Surprisingly, when the content of JP-10 was higher, the freezing point of blends comprising HOBT4 and JP-10 revealed a remarkable synergistic effect: the freezing points of the blends were lower than those of the individual fuels.

Flash point

The flash point defines the minimum temperature at which a flammable fuel can ignite or flash when in contact with a spark or flame [46]. Vaporizing liquids below the flashpoint also does not provide enough support for combustion. Consequently, the flash point is vital for storing and transporting liquid fuels. Liquids with flash points lower than 37.8 °C or higher than 37.8 °C are flammable or combustible [47]. Lower flash points pose a risk for storing and transporting the fuel. Therefore, ASTM D1655 and ASTM D7566 set the required minimum flash point at 38 °C.

The hydrogenation of OBT increased its kinematic viscosity, which affected the fuel's atomization and, consequently, the flash point of HOBT. Fig. S12a showed that the flash point of HOBT increases as the hydrogenation rate increases, from 37.3–42.8 °C, a rise of 14.7%, when the hydrogenation rate is higher than 20% has reached the standard requirements. Fig. S12b shows that the flash point of the blended biomass fuel decreased linearly with the addition of HOBT. However, the addition of 20% HOBT had a negligible effect on the flash point of the blended biomass fuel. Overall, the flash points of HOBT4 and the blended biofuels at all ratios met the minimum flash point requirements specified in the standard.

Conclusion

Non-precious metal Ni/c-MWCNT catalyst via over-impregnation was used to hydrogenate OBT. The reaction conditions of hydrotreatment of OBT were explored, and the optimal conditions were as follows: catalyst dosage of 5%, temperature of 145 °C, pressure of 3 MPa, and time of 1 h. Under the same conditions, the hydrogenation rate of 5 wt% Pd/C catalyst was only 92.8%, which was lower than 99.1% for Ni/c-MWCNT.

After hydrogenation, the smoke point of the HOBT increased by 36.3%, the calorific value increased by 3.2%, and the flash point increased by 14.7% compared to its pre-hydrogenation state. The HOBT had a density, flashpoint, and freezing point in line with ASTM D7566 standards. Renewable bio-based jet fuels with properties comparable to or even better than the freezing point of JP-10 can be prepared when the content of HOBT reaches 20%.

Blended biomass fuel was synthesized by blending HOBT with JP-10 in varying proportions (20%, 40%, 60%, 80%). The fuel properties of the blends were assessed using the ASTM standard for kinematic viscosity, calorific value, density, flash point, smoke point, and freezing point. The density and flash point of the blended biomass fuel after compounding tended to decrease linearly with increasing percentage of HOBT, while the opposite was true for viscosity. A synergistic effect was observed for the freezing point of the blended biomass fuels. In contrast, an inverse synergistic effect was observed for the smoke point when the percentage of HOBT in the blended biomass fuels reached 20% and 40%.

Supplementary Information The online version contains supplementary material available at https://doi.org/10.1007/s11144-024-02639-5.

Acknowledgements This work was supported by the National Natural Science Foundation of China (Grant Nos. 22368006, 32160349), Guangxi Natural Science Foundation (Grant No. 2024GXNSFAA999185), Guangxi Key Laboratory of Petrochemical Resource Processing and Process Intensification Technology (Grant No. 2022Z002).

Data availability Not available

Declarations

Competing interest The authors declare that they have no known competing financial interests or personal relationships that could have appeared to influence the work reported in this paper.

References

1. Muldoon JA, Harvey BG (2020) Bio-based cycloalkanes: The missing link to high-performance sustainable jet fuels. Chemsuschem 13:5777–5807
2. Zou JJ, Zhang XW, Pan L (2020) High-energy-density fuels for advanced propulsion: Design and synthesis. Wiley, Hoboken
3. Ezekannagha CB, Onukwuli OD, Uzoh CF, Eze CN (2023) Kinetic modeling of bio-based heterogeneously catalyzed lard oil methanolysis in methyl ester production. React Kinet Mech Catal 136:2617–2638
4. Rana AK, Guleria S, Gupta VK, Thakur VK (2023) Cellulosic pine needles-based biorefinery for a circular bioeconomy. Bioresour Technol 367:128255
5. Yi M, Jia T, Dong LM, Zhang L, Leng CH, Liu SY, Lai M (2021) Resin yield in Pinus elliottii Engelm. is related to the resin flow rate, resin components and resin duct characteristics at three locations in southern China. Ind Crops Prod 160:113141
6. Golets M, Ajaikumar S, Mikkola JP (2015) Catalytic upgrading of extractives to chemicals: monoterpenes to "EXICALS." Chem Rev 115:3141–3169
7. Karthikeyan R, Mahalakshmi N (2007) Performance and emission characteristics of a turpentine–diesel dual fuel engine. Energy 32:1202–1209
8. Arpa O, Yumrutas R, Alma MN (2010) Effects of turpentine and gasoline-like fuel obtained from waste lubrication oil on engine performance and exhaust emission. Energy 35:3603–3613

9. Umar S, Abdelmalik AA, Sadiq U (2018) Synthesis and characterization of a potential bio-based dielectric fluid from neem oil seed. Ind Crops Prod 115:117–123
10. Gao Z, Zou XY, Huang Z, Zhu L (2019) Predicting sooting tendencies of oxygenated hydrocarbon fuels with machine learning algorithms. Fuel 242:438–446
11. Musthafa B, Asokan M (2024) Reducing NOx emission from palm biodiesel/diesel blends in CI engine: a comparative study of cetane improvement techniques through hydrogenation and fuel additives. P I Mech Eng. https://doi.org/10.1177/09544089231223380
12. Wadumesthrige K, Salley SO, Ng KS (2009) Effects of partial hydrogenation, epoxidation, and hydroxylation on the fuel properties of fatty acid methyl esters. Fuel Process Technol 90:1292–1299
13. Mondal K, Lalvani S (2008) Low temperature soybean oil hydrogenation by an electrochemical process. J Food Eng 84:526–533
14. Donoso D, Garcia D, Ballesteros R, Lapuerta M, Canoira L (2021) Hydrogenated or oxyfunctionalized turpentine: options for automotive fuel components. RSC Adv 11:18342–18350
15. Lapuerta M, Rodríguez-Fernández J, Ramos Á, Donoso D, Canoira L (2023) Hydrogenated terpenic renewable fuels: emissions and combustion analysis. Renew Energ 208:152–161
16. Vallinayagam R, Vedharaj S, Yang WM, Lee PS, Chua KJE, Chou SK (2013) Combustion performance and emission characteristics study of pine oil in a diesel engine. Energy 57:344–351
17. Yang XK, Uddin MH, Zhou XP, Neupane B, Miller GC, Coronella CJ, Poulson SR, Lin HF (2018) Production of high-density renewable aviation fuel from arid land crop. ACS Sustain 6:10108–10119
18. Liu LJ, Lou H, Chen M (2016) Selective hydrogenation of furfural to tetrahydrofurfuryl alcohol over Ni/CNTs and bimetallic CuNi/CNTs catalysts. Int J Hydrogen Energ 41:14721–14731
19. Tessonnier JP, Pesant L, Ehret G, Ledoux MJ, Pham-Huu C (2005) Pd nanoparticles introduced inside multi-walled carbon nanotubes for selective hydrogenation of cinnamaldehyde into hydrocinnamaldehyde. Appl Catal A-Gen 288:203–210
20. Lin M, Yan YH, Li XX, Li R, Wu YL (2024) Hydrothermal hydrogenation/deoxygenation of palmitic acid to alkanes over Ni/activated carbon catalyst. Chin J Chem Eng 66:8–18
21. Yousefi SR, Ghanbari D, Salavati-Niasari M, Hassanpour M (2016) Photo-degradation of organic dyes: simple chemical synthesis of $Ni(OH)_2$ nanoparticles, $Ni/Ni(OH)_2$ and Ni/NiO magnetic nanocomposites. J Mater 27:1244–1253
22. Zhang ZN, Liu CW, Liu D, Shang YN, Yin XQ, Zhang P, Mamba BB, Kuvarega AT, Gui JZ (2020) Hydrothermal carbon-supported Ni catalysts for selective hydrogenation of 5-hydroxymethylfurfural toward tunable products. J MATER SCI 55:14179–14196
23. Koyuncu DDE, Ozben N, Oktar N, Murtezaoglu K (2023) Decomposition of formic acid over Ni-containing SiO_2 catalysts synthesized by various one-pot synthesis routes. React Kinet Mech Catal 136:2569–2586
24. Ding L, Rahimi P, Hawkins R, Bhatt S, Shi Y (2009) Naphthenic acid removal from heavy oils on alkaline earth-metal oxides and ZnO catalysts. APPL CATAL A-GEN 371:121–130
25. Sharghi H, Aberi M, Doroodmand MM (2008) Reusable cobalt(III)-salen complex supported on activated carbon as an efficient heterogeneous catalyst for synthesis of 2-arylbenzimidazole derivatives. Adv Synth 350:2380–2390
26. Wei QL, Chen XP, He YJ, Fu JW, Liang JJ, Wei XJ, Wang LL (2022) Ni nanoparticles supported on N-doped carbon nanotubes for efficient hydrogenation of C5 hydrocarbon resins under mild conditions. Microporous Mesoporous Mater. 333:111727
27. Yang GJ, Han T, Lu XJ, Yi JH, Tan SL, Fang D (2022) "Powder electrodeposition" synthesis of NiO-Ni/CNTs composites with high performances of lithium storage battery. J Alloys Compd 898:163005
28. Wang XY, Jia TH, Pan L, Liu Q, Fang YM, Zou JJ, Zhang XW (2021) Review on the relationship between liquid aerospace fuel composition and their physicochemical properties. Trans Tianjin Univ 27:87–109
29. Demko J, Machava J (2022) Tree resin, a macroergic source of energy, a possible tool to lower the rise in atmospheric CO_2 levels. Sustainability 14:3506
30. Blakey S, Rye L, Wilson CW (2011) Aviation gas turbine alternative fuels: a review. Proc Combust Inst 33:2863–2885
31. Woodroffe J-D, Lupton DV, Garrison MD, Nagel EM, Siirila MJ, Harvey BG (2021) Synthesis and fuel properties of high-energy density cyclopropanated monoterpenes. Fuel Process Technol 222:106952

32. Li YL, Xu XL, Niu MM, Chen J, Wen JH, Bian H, Yu C, Liang M, Ma L, Lai F, Liu XM (2019) Thermal stability of abietic acid and its oxidation products. Energy Fuels 33:11200–11209
33. Liu Y, Wang XP, Chen C, Li L, Yu HL, Wu Q, Xie CX, Yu ST, Liu SW (2018) Hydrogenation of rosin to hydrogenated rosin by Ru/Fe_3O_4@C magnetic catalyst. Catal Lett 148:3147–3157
34. Huang YY, Chen XP, Deng YF, Zhou D, Wang LL (2015) A novel nickel catalyst derived from layered double hydroxides (LDHs) supported on fluid catalytic cracking catalyst residue (FC3R) for rosin hydrogenation. Chem Eng J 269:434–443
35. Shaefer W (1930) Quantitative hydrogenation of the principal unsaturated components of turpentine, pine oil, and rosin. Ind Eng Chem Anal Ed 2:115–117
36. Zhu JQ, Alegre-Requena JV, Cherry P, Curtis D, Jabed MA, Kim S, Mcenally CS, Pfefferle LD, Woodroffe JD (2023) Sooting tendencies of terpenes and hydrogenated terpenes as sustainable transportation biofuels. Proc Combust Inst 39:877–887
37. Eller ZN, Varga ZN, HancsóK J (2019) Renewable jet fuel from kerosene/coconut oil mixtures with catalytic hydrogenation. Energy Fuels 33:6444–6453
38. Wang WY, Zhang XH, Jiang ZJ, Cui YY, Kang QX, Zhao XL, Zhang Q, Ma LL (2022) Controllably produce renewable jet fuel with high-density and low-freezing points from lignocellulose-derived cyclopentanone. Fuel 321:124114
39. Wilbon PA, Chu F, Tang C (2013) Progress in renewable polymers from natural terpenes, terpenoids, and rosin. Macromol Rapid Commun 34:8–37
40. Braun-Unkhoff M, Kathrotia T, Rauch B, Riedel U (2015) About the interaction between composition and performance of alternative jet fuels. CEAS Aeronaut 7:83–94
41. Ramírez-Verduzco LF, Rodríguez-Rodríguez JE, Jaramillo-Jacob ADR (2012) Predicting cetane number, kinematic viscosity, density and higher heating value of biodiesel from its fatty acid methyl ester composition. Fuel 91:102–111
42. Yue L, Li GQ, He GJ, Guo YS, Xu L, Fang WJ (2016) Impacts of hydrogen to carbon ratio (H/C) on fundamental properties and supercritical cracking performance of hydrocarbon fuels. Chem Eng J 283:1216–1223
43. Benavides A, Benjumea P, Cortés FB, Ruiz MA (2021) Chemical composition and low-temperature fluidity properties of jet fuels. Processes 9:1184
44. Zhang XK, Li N, Han S, Wei Z, Dai B (2022) Terpene resin prepared from renewable turpentine oil as a new type of cold flow improver for soybean biodiesel-diesel blends. Fuel 320:123844
45. Dhar Dubey KK, Jeyaseelan C, Upadhyaya KC, Chimote V, Veluchamy R, Kumar A (2020) Biodiesel production from Hiptage benghalensis seed oil. Ind Crops Prod 144:112027
46. Phoon LY, Mustaffa AA, Hashim H, Mat R (2014) A review of flash point prediction models for flammable liquid mixtures. Ind Eng Chem Res 53:12553–12565
47. Poor HM, Sadrameli SM (2017) Calculation and prediction of binary mixture flash point using correlative and predictive local composition models. Fluid Phase Equilib 440:95–102